RSC Advances

PAPER

View Article Online
View Journal | View Issue

Cite this: *RSC Adv.*, 2023, **13**, 33675

Energy transfer mechanisms and color-tunable luminescence of $Tm^{3+}/Tb^{3+}/Eu^{3+}$ co-doped $Sr_4Nb_2O_9$ phosphors for high-quality white light-emitting diodes

Ravina,[a] Kanishk Poria,[b] Mukesh K. Sahu,[c] A. Kumar,[a] Anu,[d] Sajjan Dahiya,[e] Nisha Deopa *[a] and A. S. Rao[d]

This paper investigates the synthesis and luminescence characteristics of $Tm^{3+}/Tb^{3+}/Eu^{3+}$ co-doped $Sr_4Nb_2O_9$ (SNB) phosphors as potential candidates for white light-emitting diodes (WLEDs). The study explores the energy transfer mechanisms and color-tunable characteristics of these phosphors. The SNB phosphors were prepared using a solid-state reaction method, and their structural and morphological properties were characterized using X-ray diffraction (XRD), scanning electron microscopy (SEM), energy-dispersive X-ray spectroscopy (EDS), and Fourier-transform infrared (FT-IR) spectroscopy. The diffuse reflectance, photoluminescence (PL) and time resolved photoluminescence (TRPL) properties were investigated, revealing efficient energy transfer processes from Tm^{3+} to Tb^{3+} and Eu^{3+} ions. The energy transfer mechanisms were determined through critical distance calculations and analysis of multipolar interactions. The co-doped phosphors exhibited tunable emission colors ranging from blue to white light, with controllable correlated color temperatures (CCTs) and high color rendering indices (CRIs). The CIE chromaticity coordinates were optimized to approach neutral white light. The PL intensity is maintained at 81.19% at 150 °C of that of room temperature which showcases the remarkable thermal stability of the as-prepared phosphors. The results highlight the potential of $Tm^{3+}/Tb^{3+}/Eu^{3+}$ co-doped SNB phosphors for generating high-quality, color-tunable white light for advanced lighting applications.

Received 14th August 2023
Accepted 8th November 2023

DOI: 10.1039/d3ra05519a

rsc.li/rsc-advances

1 Introduction

With technological advancements, especially the widespread utilization of rare earth ion-doped phosphors, white light-emitting diodes (WLEDs) have progressively emerged as the optimal choice for next-generation lighting solutions. This preference arises from their inherent advantages, including cost-effectiveness, high efficiency, and environmental friendliness.[1–3] Currently, white light can be achieved through two approaches. The first involves integrating a blue InGaN chip with YAG:Ce^{3+} yellow phosphors. However, this approach lacks the red segment of the spectrum, leading to a diminished color rendering index (CRI) and an elevated correlated color temperature (CCT). This deviation from the natural white light region poses a challenge to achieving high-quality white light illumination. Another approach involves using a near-ultraviolet chip combined with three-color phosphors. This method is capable of meeting the requirements for a high color rendering index (CRI) and achieving a suitable correlated color temperature (CCT).[4] By employing this approach, it becomes possible to produce white light that closely resembles natural lighting conditions. Therefore, the development of color-tunable phosphors on a single-phase substrate is a highly significant research direction within the field of white light-emitting diodes (WLEDs). This approach aims to create phosphors that can be adjusted to produce a wide range of colors, enabling versatile and customizable lighting solutions.

Rare-earth ions exhibit a remarkably diverse electronic structure, rendering them capable of emitting photoluminescence across a wide range of wavelengths, including visible and infrared light. Particularly in the visible light region, their emission ability and vivid colors stand out, making rare-earth ions highly desirable for various applications, such as lighting and display technologies.[5] The fusion of three primary colors—red, green, and blue—is well-known to yield white light.

[a]*Department of Physics, Chaudhary Ranbir Singh University, Rohtak Bypass Road, Jind-126102, Haryana, India. E-mail: nispectro999@gmail.com; Tel: +918860551723*
[b]*Department of Physics, Panjab University, Chandigarh-160014, India*
[c]*School of Computing, Graphic Era Hill University, Haldwani, Uttarakhand-263136, India*
[d]*Department of Applied Physics, Delhi Technological University, Bawana Road, New Delhi-110 042, India*
[e]*Department of Physics, Maharshi Dayanand University, Rohtak-124001, Haryana, India*

In this context, different phosphors utilize Tm^{3+}, Eu^{3+}, and Tb^{3+} ions as blue, red, and green emitters, respectively. These ions are chosen for their abundant electron transitions, contributing to the emission properties of the phosphors. For instance, Tm^{3+} doping in inorganic compounds often yields excellent blue-emitting performance due to the blue transition from $^1D_2 \rightarrow {}^3F_4$.[6,7] Eu^{3+} ions emit in the orange-red region of the spectrum through the $^5D_0 \rightarrow {}^7F_J$ ($J = 0$–4) transitions,[8,9] while Tb^{3+} ions are commonly used as blue-green emitters with the $^5D_4 \rightarrow {}^7F_J$ ($J = 6$–3) transitions.[10] Co-doping Tm^{3+}, Eu^{3+}, and Tb^{3+} ions into a single host material allows for the potential generation of a single-phased phosphor emitting white light.[11] This approach permits the generation of white light by combining emissions from these different ions. Furthermore, the selection of an appropriate host material is vital for synthesizing phosphors with high performance. The host material plays a crucial role by providing suitable crystal fields for the activator ions. The crystal structure and properties of the host material significantly influence the luminescent properties and efficiency of the phosphor. Hence, careful consideration and optimization of the host material are essential to achieve phosphors with desirable performance characteristics.

The extensive study of niobate group materials is driven by their remarkable electro-optic, dielectric, ferroelectric, pyroelectric, and piezoelectric properties.[12,13] Niobate serves as a highly favorable host matrix for doping rare-earth ions due to its exceptional luminescent properties, excellent chemical stability, and good thermal stability. Concerning characteristics related to light emission, the optical absorption observed in niobates is attributed to charge transfer occurring within the NbO_6 complex.[14] This absorption behavior significantly influences their luminescent properties. While certain pure niobates may not exhibit luminescence, substantial research has been conducted on rare-earth-doped niobates due to their potential as light-emitting materials. The incorporation of rare-earth ions into niobate structures allows for the creation of luminescent centers, expanding the range of applications in areas such as lighting, displays, and optoelectronics.

2 Experimental procedure and instrumentations

Through the solid-state reaction method, we synthesized samples of strontium niobate phosphor $Sr_4Nb_2O_9$ (SNB) doped with Tm^{3+}, Tb^{3+}, and Eu^{3+}. The precursor materials $SrCO_3$ (98%), Nb_2O_5 (99.9%), Tm_2O_3 (99.9%), Tb_4O_7 (99.9%), Eu_2O_3 (99.99%) were of analytical grade. Following their precise stoichiometric ratio, we weighed and thoroughly mixed the precursors using an agate mortar until achieving uniformity. These homogeneous mixtures were then poured in an alumina crucible and sintered at 1350 °C for 7 hours, followed by gradual cooling to ambient temperature. We labeled the resulting phosphors as follows: SNB:xTm^{3+} ($x = 0.01$, 0.03, 0.05, 0.07, 0.10 mol), SNB:0.03Tm^{3+}, yTb^{3+} ($y = 0.01$, 0.02, 0.03, 0.04, 0.05, 0.06, 0.08, 0.10 mol) denoted as TT1-TT10, SNB:0.03Tm^{3+}, 0.06Tb^{3+}, zEu^{3+} ($z = 0.01$, 0.03, 0.05 and 0.07 mol) labeled as TTE1-TTE7. Finally, we finely powdered the prepared samples for subsequent characterization.

Structural analysis of the samples was conducted using X-ray diffraction (XRD). A Bruker D8 Advance diffractometer equipped with a nickel filter and a Cu Kα radiation source (wavelength $\lambda = 1.5406$ Å) was utilized within the 2θ range of 20° to 80°. For examination of sample morphology and elemental composition, scanning electron microscopy (SEM) and energy-dispersive X-ray spectroscopy (EDS) were performed using a Zeiss Gemini 300 instrument. Additionally, Fourier-transform infrared (FT-IR) spectra of the as-synthesized samples were recorded using a Nicolet IS50 FT-IR apparatus. UV spectrum analysis was conducted using a Jasco V-770 spectrophotometer with light sources of deuterium and halogen and a resolution of 1.0 nm. For validation of PL excitation and emission spectra, a Jasco 8300 FP spectrofluorophotometer employing 300 W xenon lamp acts as excitation source and a resolution of 1.0 nm was used. PL decay measurements were performed using the Hitachi F 7000 spectrofluorometer in conjunction with a 450 watts microsecond xenon flash lamp. The time-resolved photoluminescence (TDPL) was performed using the FLAME-S-XR1-ES Ocean Optics spectrometer along with a sample holder along with a heating assembly.

3 Results and discussion

3.1. Study of XRD pattern

Fig. 1 presents the XRD patterns of SNB phosphors doped with 3 mol% Tm^{3+}, 3 mol% Tm^{3+} and 6 mol% Tb^{3+}. The diffraction patterns demonstrate consistency with standard data (Card No. 048-0558), confirming the successful incorporation of Tm^{3+}, Tb^{3+} and Eu^{3+}ions into the host lattice. The XRD patterns confirm that the as-prepared phosphor possesses a crystalline cubic structure within the *Fm*3*m* space group, showing no structural alterations.[15] The impurities at 28° and 50° in the XRD is because of the difference between both ionic radius and charge numbers between the Ln^{3+} ions and Sr^{2+} ions. The average crystallite sizes (D) were calculated using Debye–Scherer equation (eqn (1)) from the literature,[16]

$$D = \frac{K\lambda}{\beta \cos \theta} \quad (1)$$

resulting in values of 41.64 nm for SNB:3 mol% Tm^{3+}, 40.61 nm for SNB:3 mol% Tm^{3+} and 6 mol% Tb^{3+}, and 41.07 nm for SNB:3 mol% Tm^{3+}, 6 mol% Tb^{3+}, and 5 mol% Eu^{3+}.

Fig. 2 demonstrates the XRD patterns of the SNB:3Tm^{3+}/6Tb^{3+}/zEu^{3+} (z = 1, 3, 5 and 7 mol%) samples which are consistent with the standard data. The average crystallite size were evaluated and found to be 42.26, 41.88, 41.07 and 42.12 nm, respectively.

3.2. SEM and EDS studies

SEM imaging, SEM-EDS mapping, and EDS spectrum analysis were employed to investigate the morphology and elemental composition of the SNB sample doped with 3 mol% Tm^{3+} and 1 mol% Tb^{3+}, as illustrated in Fig. 3. In Fig. 3(a), the SEM image

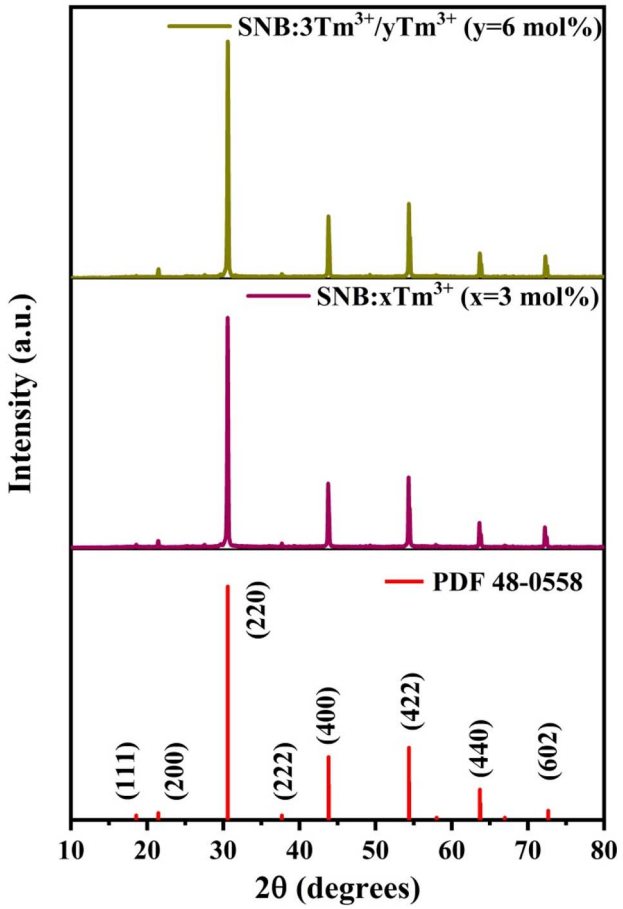

Fig. 1 XRD patterns of SNB:xTm^{3+} (x = 3 mol%), SNB:3Tm^{3+}/yTb^{3+} (y = 6 mol%) samples and compared with standard data.

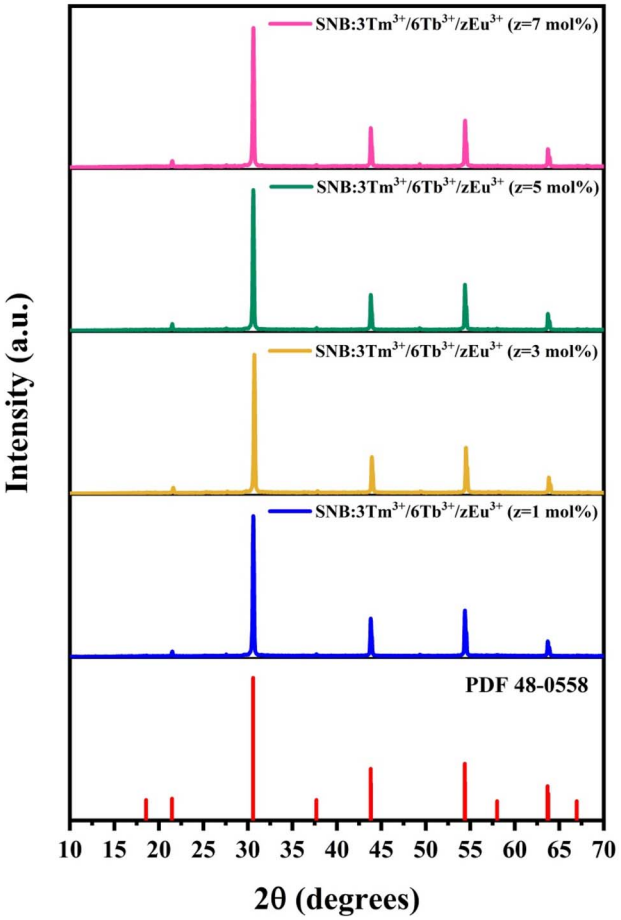

Fig. 2 XRD patterns of SNB:3Tm^{3+}/6Tb^{3+}/zEu^{3+} (z = 1, 3, 5 and 7 mol%) samples and compared with standard data.

unveils the presence of regular and smooth micron-sized particles within the SNB sample. Elemental mapping results in Fig. 3(b–f) exhibit a uniform distribution of Sr, Nb, O, Tm, and Tb elements across the grains. The EDS spectrum depicted in Fig. 3(g) displays distinct peaks corresponding to Nb, O, and Sr, along with smaller peaks representing Tm and Tb. No indications of impurity elemental peaks are evident, indicating the successful integration of Tm^{3+} and Tb^{3+} ions into the SNB host matrix. The inset within Fig. 3(g) illustrates the elemental compositions.

3.3. FTIR studies

The structural components and functional groups present in the as-synthesized SNB:xTm^{3+} (x = 1, 3, 5, 7, and 10 mol%) phosphor were analyzed by recording FT-IR spectra in the wavenumber range of 4000–400 cm^{-1}. Fig. 4 illustrates the FT-IR spectra of the synthesized phosphor. FT-IR spectroscopy was employed in the initial stage of material analysis to ensure the quality of the product. The shift in peak positions indicated the presence of contaminants. The spectra exhibited analogous positions of shoulder, as shown in Fig. 4. The FT-IR spectra revealed the presence of nine peaks at approximately 418, 435, 525, 651, 861, 1442, 2885, 2948, and 2989 cm^{-1}. These peaks were assigned based on previous reported papers. The peak observed near 418 and 525 cm^{-1} corresponds to the Sr–O stretching modes.[17] The peaks around 435 and 861 cm^{-1} are attributed to the coupling between Nb–O stretching mode.[18] The peak at approximately 651 cm^{-1} is due to Tm–O stretching vibrations.[19] The peaks observed in the range of 1442 and 2989 cm^{-1} are associated with water molecules.[20] The disturbances in the form of peaks between 1000 to 3000 cm^{-1} may indicate the presence of residual organic compounds.[21] Furthermore, the absence of significant evidence of carbonates or carboxyl groups in the FT-IR spectra confirms the synthesis of phosphor materials from their precursor carbonates.

3.4. Diffuse reflectance study

Diffuse reflectance spectra were collected for the SNB samples doped with 3 mol% Tm^{3+} and SNB:3 mol% Tm^{3+}, 6 mol% Tb^{3+} over the wavelength range of 200–1800 nm, spanning the UV-visible and near-IR regions at room temperature, as depicted in Fig. 5.

In the phosphors doped solely with Tm^{3+}, the absorption bands located at approximately 684, 788, 1216, and 1644 nm

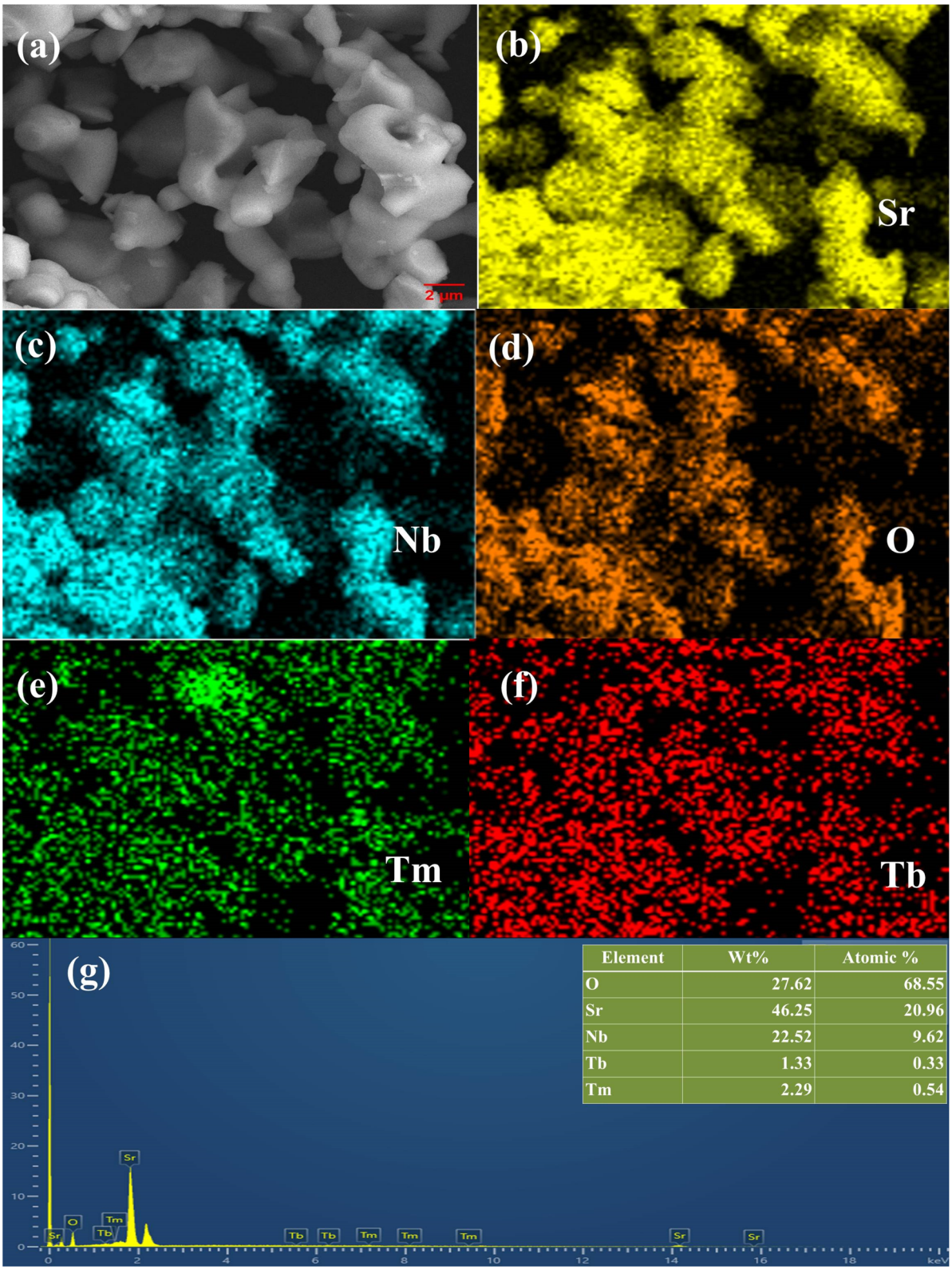

Fig. 3 (a) SEM images. (b–f) SEM-EDS mapping. (g) EDS spectrum of SNB:3 mol% Tm^{3+}, 6 mol% Tb^{3+} phosphor [inset shows the elements weight and atomic percent].

correspond to transitions from the ground level $^3H_6$ to $^3F_3$, $^3H_4$, $^3H_5$ and $^3F_4$ levels, respectively.[22] In phosphors co-doped with both Tm^{3+} and Tb^{3+}, a captivating interplay of energy level transitions is observable. Tm^{3+} ions exhibit transitions at 684, 788, 1216, and 1644 nm, while Tb^{3+} ions exhibits the $^7F_6 \rightarrow {}^5D_3$ energy level transition at 386 nm.[23]

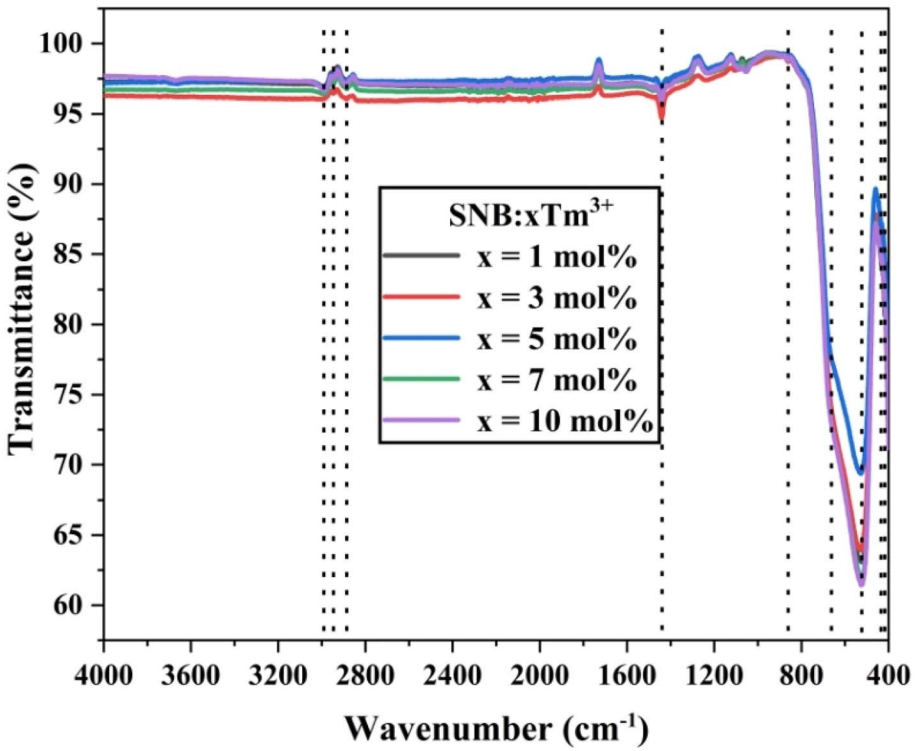

Fig. 4 FT-IR spectra of SNB:xTm^{3+} samples.

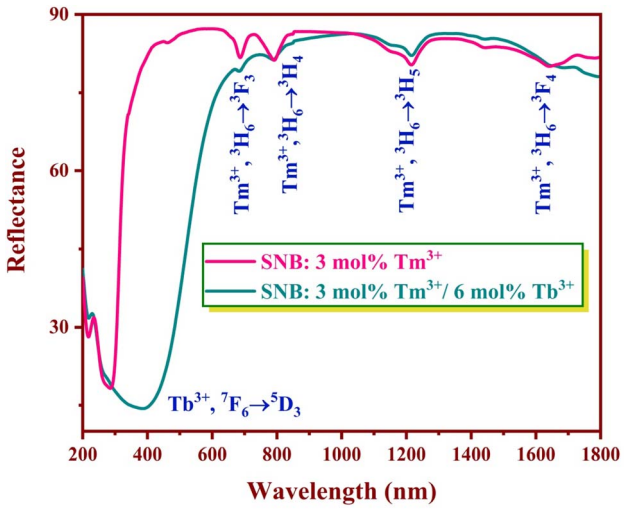

Fig. 5 Diffuse reflectance spectra of SNB:3 mol% Tm^{3+} and SNB:3 mol% Tm^{3+}, 6 mol% Tb^{3+} phosphors.

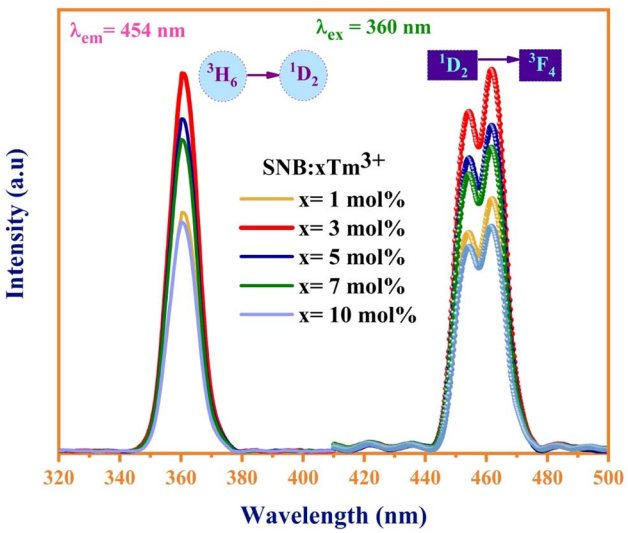

Fig. 6 PLE and PL spectra of SNB:xTm^{3+} phosphors.

3.5. Photoluminescence properties

Fig. 6 displays the photoluminescence excitation and emission spectra of the synthesized SNB:xTm^{3+} (x = 1, 3, 5, 7, 10 mol%) phosphors. The dominant excitation peak at 360 nm can be attributed to the distinctive $^3H_6 \rightarrow {}^1D_2$ transitions of Tm^{3+} ions, effectively stimulated by near-ultraviolet (NUV) light. In the emission spectra, a broad peak ranging from 440 to 480 nm under the 360 nm excitation for SNB:xTm^{3+} (x = 1, 3, 5, 7, 10) phosphors is associated with the $^1D_2 \rightarrow {}^3F_4$ transition.[24]

Interestingly, the peak intensity of the samples initially increases and then diminishes as the Tm^{3+} doping concentration rises. This intensity attains its peak at x = 3 mol%, which is attributed to concentration quenching, as depicted in Fig. 6. This phenomenon arises from the cross relaxation mechanism due to variations in the spacing between luminescence centers. At lower concentrations of Tm^{3+} ions, the spacing between them is sufficiently small to effectively neglect fluorescence quenching.[25] However, with an increasing concentration of Tm^{3+} ions,

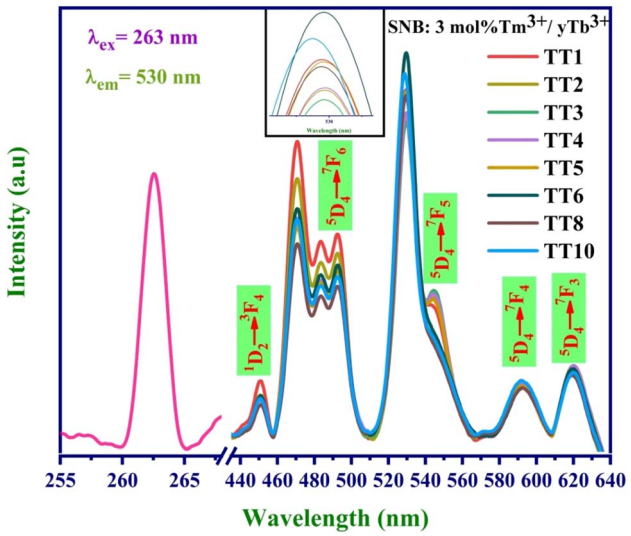

Fig. 7 PLE and PL spectra of SNB:3 mol% Tm^{3+}/yTb^{3+} phosphors.

the gap between the ions diminishes, falling below the critical transfer distance. This results in a higher utilization of Tm^{3+} ions at the $^1D_2$ level, consequently leading to a decrease in luminous efficiency.

3.6. Energy transfer from Tm^{3+} to Tb^{3+}

To explore the energy transfer mechanism from Tm^{3+} to Tb^{3+} ions, we prepared SNB phosphors doped with 3 mol% Tm^{3+} and varying concentrations of Tb^{3+} (denoted as y mol%, where $y = 1$, 2, 3, 4, 5, 6, 8, and 10 mol%). Fig. 7 illustrates the emission spectra under 263 nm UV light excitation, and a spectral comparison reveals that the emission peak positions remain nearly consistent across the 8 samples, appearing at approximately 450, 492, 530, 591, and 620 nm.[26]

Analysis of the emission spectra indicates that as the concentration of Tb^{3+} ions increases, the luminescent intensity of the distinct blue emission peak at 450 nm decreases. Meanwhile, the emission peaks attributed to Eu^{3+} ions at 530 nm initially experience an increase, reaching a maximum for Tm-3 mol% and Tb-6 mol%, followed by a gradual decrease. This observation suggests the occurrence of a concentration quenching phenomenon, signifying the energy transfer from Tm^{3+} to Tb^{3+} ions.

The efficiency of energy transfer from Tm^{3+} to Tb^{3+} ions can be quantified using the formula:[27]

$$\eta = 1 - \frac{I_T}{I_T + I_D} \quad (2)$$

In this equation, I_T and I_D denote the photoluminescence intensities of the emission peaks at 450 and 530 nm, respectively.

The calculated efficiency values for the TT1, TT2, TT3, TT4, TT5, TT6, TT8, and TT10 phosphors are 86.1%, 88.5%, 89.7%, 90.2%, 90%, 91.3%, 90.3%, and 90.4%, respectively. These results underscore a significant improvement in energy transfer efficiency with increasing concentration, reaching its peak value in the TT6 phosphor sample. The higher concentration of Tb^{3+} ions surrounding the Tm^{3+} ions promotes a greater likelihood of cross relaxation between the transitions of Tm^{3+} ($^1D_2 \rightarrow {}^3F_4$) and Tb^{3+} ($^5D_4 \rightarrow {}^7F_5$).[28] This phenomenon elucidates the concentration quenching and the reduction in emission intensity at 450 nm. The quantum yield for the TT6 phosphor was evaluated using the equations mentioned in literature and comes out to be 41% which is higher than the other reported works.[29,30]

Fig. 8 graphically portrays the energy transfer efficiency between Tm^{3+} and Tb^{3+} ions, alongside the emission intensities corresponding to the $^1D_2 \rightarrow {}^3F_4$ transition of Tm^{3+} and the $^5D_4$

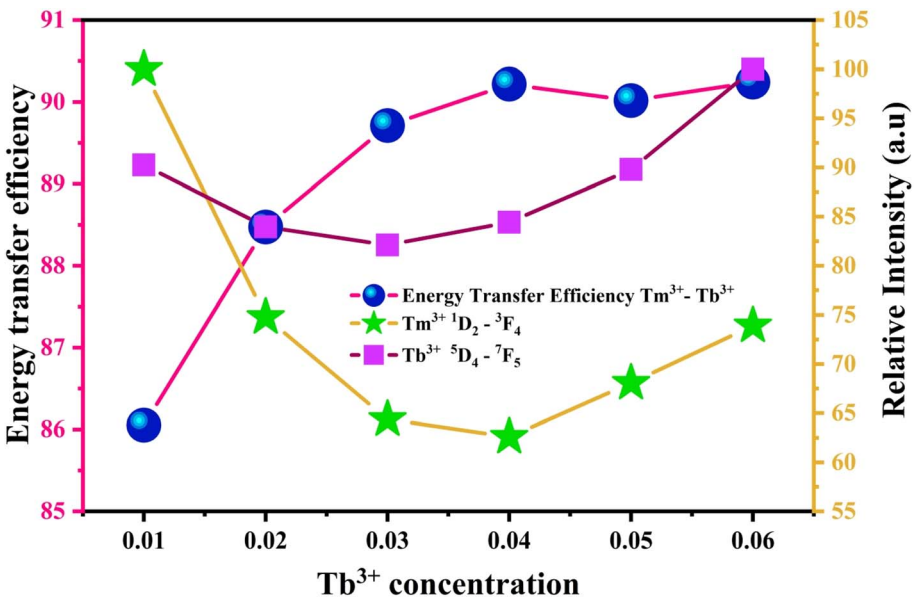

Fig. 8 Energy transfer efficiency of $Tm^{3+} \rightarrow Tb^{3+}$ and the luminous intensity curve of the monitoring wavelength were 450 nm (Tm^{3+}) and 530 nm (Tb^{3+}).

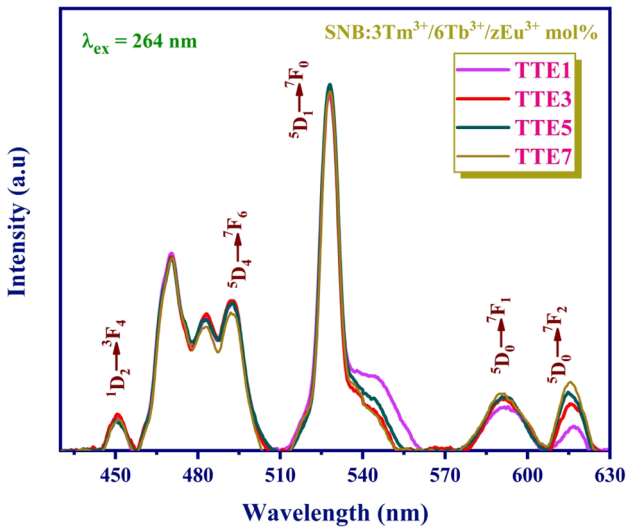

Fig. 9 PL spectra of SNB:3 mol% Tm^{3+}/6 mol% Tb^{3+}/*z* mol% Eu^{3+} phosphors under 264 nm excitation wavelength.

→ $^7F_5$ transition of Tb^{3+}. As the concentration of Tb^{3+} ions increases, the emission intensity of Tm^{3+} decline, while conversely, the emission intensity of Tb^{3+} and the energy transfer efficiency increases.

The emission spectra of SNB:3 mol% Tm^{3+}, 6 mol% Tb^{3+}, and *z* mol% Eu^{3+} phosphors illuminated by 264 nm UV light are depicted in Fig. 9. These spectra reveal distinct emission peaks associated with Tm^{3+}, Tb^{3+}, and Eu^{3+} ions at 450, 493, 528, 593, and 618 nm.[31,32] Notably, the positions of these characteristic peaks remain largely consistent across varying Eu^{3+} concentrations. Specifically, the emission intensity at 528 nm initially increases until the TTE5 phosphor, after which it diminishes with higher Eu^{3+} ion concentrations.

Fig. 10 provides further insight, illustrating changes in emission intensity. The emission intensity from Tm^{3+} ions at

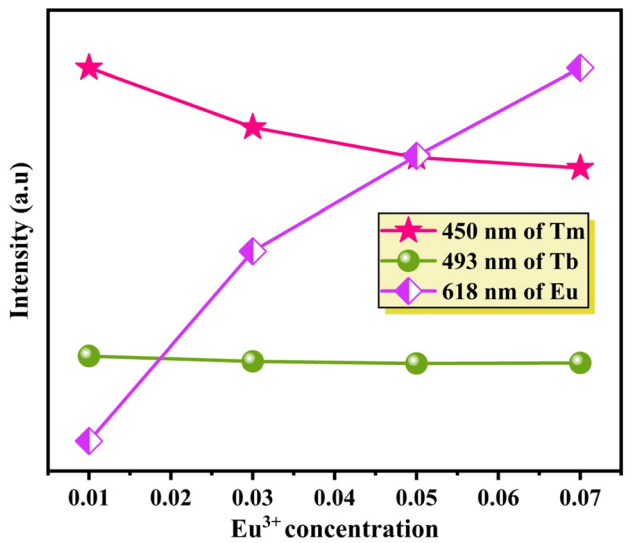

Fig. 10 Variation of the emission intensity of Tm^{3+}/Tb^{3+}/Eu^{3+} ions with the concentration of Eu^{3+} ions.

450 nm and Tb^{3+} ions at 493 nm declines, while the emission intensity attributed to Eu^{3+} ions at 618 nm rises as the Eu^{3+} concentration increases. This observation strongly implies a dual energy transfer mechanism, occurring from both Tm^{3+} and Tb^{3+} ions to Eu^{3+} ions.

Energy transfer mechanism of Tm^{3+}, Tb^{3+} and Eu^{3+} ions is illustrated in the schematic diagram presented in Fig. 11. The ions at ground state get excited to the higher energy levels of Tm^{3+}, Tb^{3+} and Eu^{3+} by the 264 nm UV excitation. After that ions gets de-excited to lower energy states $^5D_{1,0}$ of Eu^{3+} and $^5D_4$ of Tb^{3+} through non-radiative emission aided by phonons and relaxed to the ground state. In the case of Tm^{3+} ions, the blue photons emitted at 545 nm associated with $^1D_2 \rightarrow {}^3F_4$ transition. In the case of Tb^{3+} ions, the cyan and green photons emitted at 492 nm and 530 nm associated with $^5D_4 \rightarrow {}^7F_6$ transition and $^5D_4 \rightarrow {}^7F_5$ transition, respectively and for Eu^{3+} ions transitions at 593 nm ($^5D_0 \rightarrow {}^7F_1$) and 618 nm ($^5D_0 \rightarrow {}^7F_2$) emit orange and red photons, respectively. As the energy gap between the excited state $^1G_4$ of Tm^{3+} ions and $^5D_4$ of Tb^{3+} ions is smaller so they can bridge with the phonons of host lattice which results in non-radiative relaxation in Tm^{3+}. Some part of the energy is migrated to Tb^{3+} which results in transition from $^7F_6$ to $^5D_4$.[33] The non-radiative resonant energy transfer from Tm^{3+} ($^1G_4$) to Eu^{3+} ions ($^5D_2$) is because of lesser energy difference between these two states. This result in the Eu^{3+} ions transition from $^7F_1$ level to $^5D_2$ state and then return to $^5D_0$ state through non-radiatively which accompanied further radiative emission from this excited state to $^7F_1$ and $^7F_2$ state.

The energy transfer interactions between sensitizers and activators can be broadly categorized into two primary types: exchange interaction and electric multipolar interaction. The characterization of these interactions hinges on a critical parameter known as the critical distance (R_c) between the sensitizers and activators. If the value of R_c remains below 5 Å, exchange interaction is likely; however, if R_c surpasses this threshold, electric multipolar interaction becomes more probable.[34]

In order to determine the nature of the interaction between Tm^{3+} (sensitizer) and Tb^{3+} (activator), the critical distance R_c can be quantified using an equation outlined in existing literature.[35]

$$R_c = 2\left(\frac{3V}{4\pi N X_c}\right)^{\frac{1}{3}} \quad (3)$$

The computed R_c value is found to be 18.04 Å, which significantly exceeds the 5 Å threshold. This outcome strongly suggests that the energy transfer mechanism is primarily driven by electric multipolar interactions.

Utilizing Dexter's energy transfer formula for multipolar interaction and applying Reisfeld's approximation, the relationship can be presented as follows:[36,37]

$$\frac{I_{SO}}{I_S} \propto C_{Tm+Tb}^{\,n/3} \quad (4)$$

Here, I_{SO} and I_S denotes the luminescence intensities of Tm^{3+} ions without and with Tb^{3+} ions, respectively. C_{Tm+Tb} is the

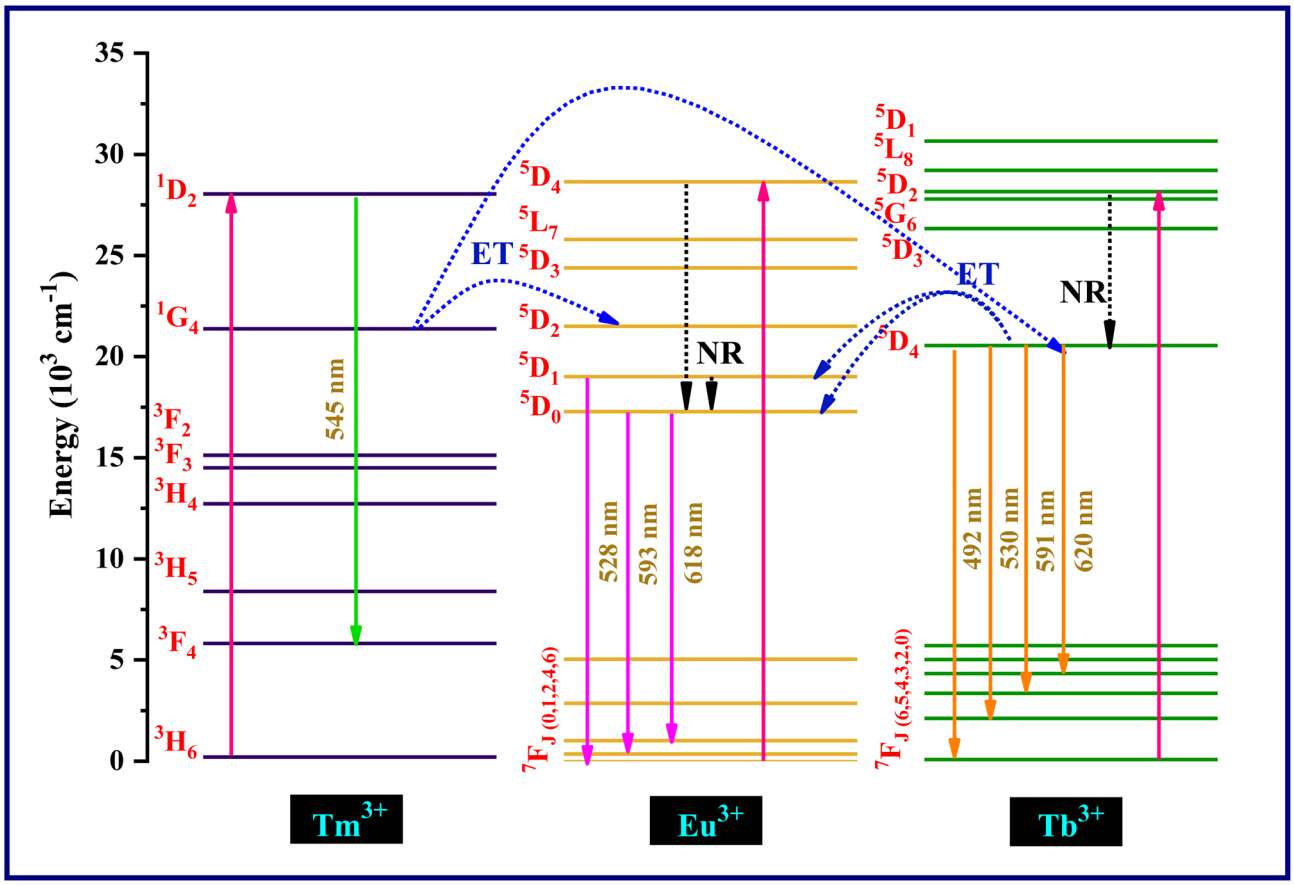

Fig. 11 Energy level diagram of $Tm^{3+}/Tb^{3+}/Eu^{3+}$ ions at 264 nm.

combined concentration of Tb^{3+} and Tm^{3+} ions. The ratio $I_{SO}/I_S \propto C_{Tm+Tb}{}^{n/3}$ with $n = 6$, 8 and 10 corresponds to different exchange interactions: dipole–dipole, dipole–quadrupole, and quadrupole–quadrupole interactions, respectively.[38] The relationship between I_{SO}/I_S and $C_{Tm+Tb}{}^{n/3}$ is illustrated in Fig. 12. It is evident that the most optimal linear fitting is observed when

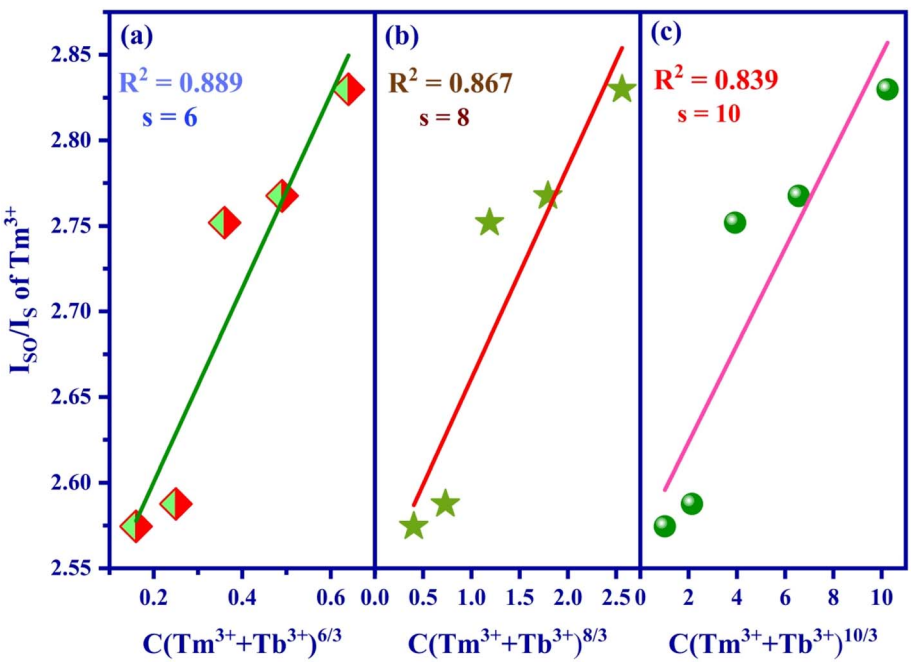

Fig. 12 Fitting relationship of I_{so}/I_s of Tm^{3+} on (a) $C\,(Tm^{3+} + Tb^{3+})^{6/3}$, (b) $C\,(Tm^{3+} + Tb^{3+})^{8/3}$ and (c) $C\,(Tm^{3+} + Tb^{3+})^{10/3}$.

$n = 6$. Consequently, the dominant mechanism for energy transfer from Tm^{3+} to Tb^{3+} is ascribed to dipole–dipole interactions.

To provide additional evidence for $Tm^{3+} \rightarrow Tb^{3+}$ energy transfer in SNB phosphor. Theoretically, it is known that when 3 mol% Tm^{3+} 6 mol% $Tb^{3+} \rightarrow z$ Eu^{3+} energy transfers, the time attenuation of Tb^{3+} ions will be accelerated energy transfer process 3 mol% Tm^{3+} 6 mol% $Tb^{3+} \rightarrow z$ Eu^{3+}. If 3 mol% Tm^{3+} 6 mol% Tb^{3+} and Eu^{3+} ions work independently without occurrence of 3 mol% Tm^{3+} 6 mol% $Tb^{3+} \rightarrow z$ Eu^{3+} energy transfers, the fluorescence lifetime of both remain equivalent to that observed in the single-doped sample. The experimental analysis of fluorescence lifetime of Eu^{3+} ions in SNB:3 mol% Tm^{3+}, 6 mol% Tb^{3+}, z Eu^{3+} phosphor was tested and the double exponential decay function was used to fit well:[39,40]

$$I(t) = I_0 + A_1 \exp\left(-\frac{t}{\tau_1}\right) + A_2 \exp\left(-\frac{t}{\tau_2}\right) \quad (5)$$

In eqn (5), I_t represents the luminous intensity at specific time t, I_0 is the background or detector zero offset. A_1 and A_2 are constants while τ_1 and τ_2 are the rapid and gradual life of exponential components, respectively. The computation of the

Table 1 Colorimetric parameters for SNB:$x$$Tm^{3+}$, SNB:3$Tm^{3+}$/$y$$Tb^{3+}$ and SNB:3Tm^{3+}/6Tb^{3+}/$z$$Eu^{3+}$ samples with excitation of 350 nm

	Color co-ordinates			
Sample	X	Y	CRI	CCT (K)
T1	0.288	0.172	—	6500
T3	0.271	0.157	—	3032
T5	0.279	0.163	—	3616
T7	0.280	0.165	—	4337
T10	0.293	0.176	—	7858
TT1	0.282	0.289	88.82	9677
TT2	0.293	0.303	89.41	8163
TT3	0.303	0.313	89.51	7256
TT4	0.302	0.314	89.52	7309
TT5	0.304	0.315	89.53	7165
TT6	0.298	0.309	89.48	7622
TT8	0.306	0.316	89.55	6984
TT10	0.302	0.312	89.45	7291
TTE1	0.299	0.307	89.34	7623
TTE3	0.298	0.303	88.87	7815
TTE5	0.301	0.307	89.11	7467
TTE7	0.299	0.303	88.64	7662

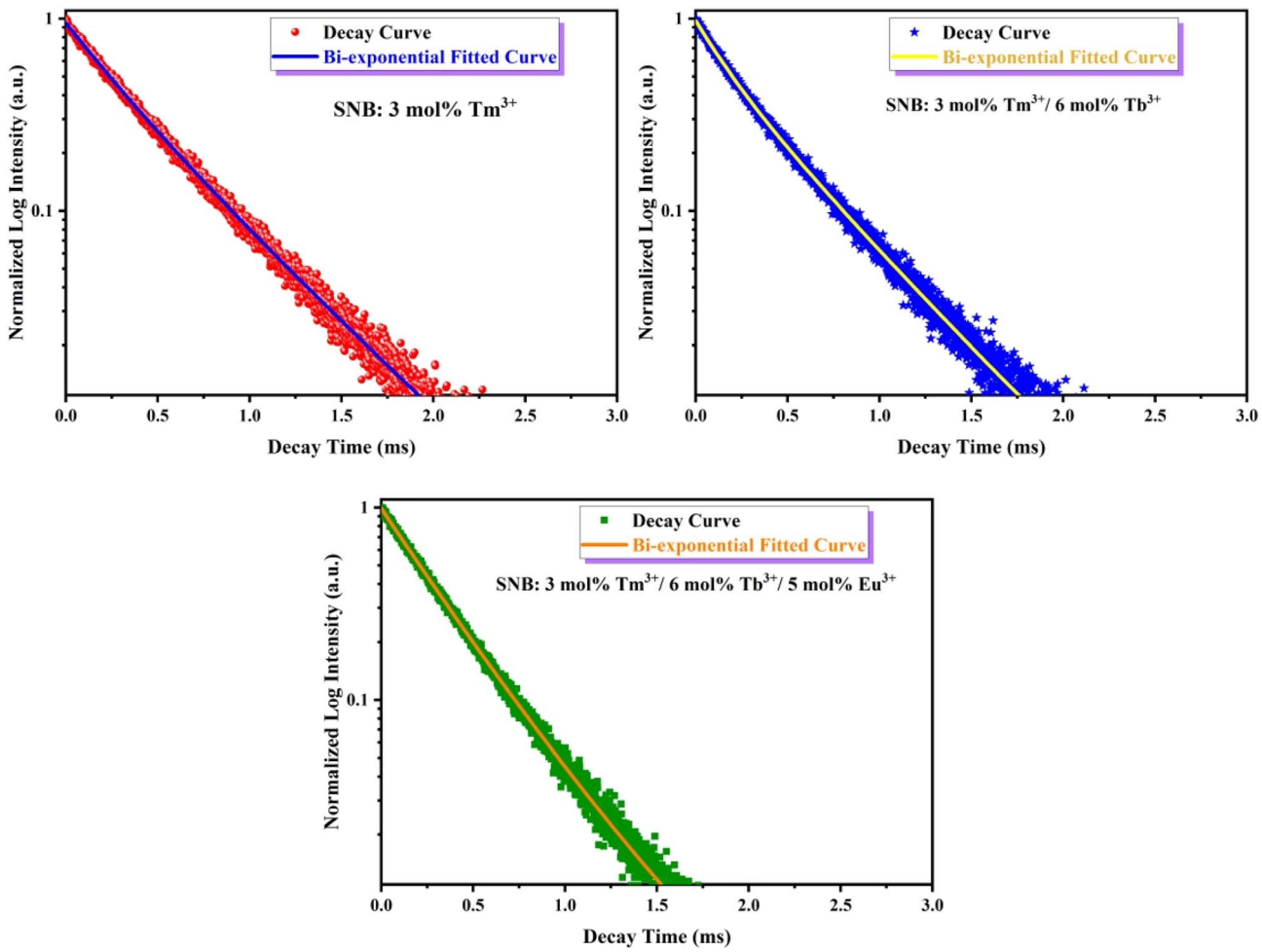

Fig. 13 PL decay curve for SNB:3 mol% Tm^{3+}, SNB:3 mol% Tm^{3+}/6 mol% Tb^{3+} and SNB:3 mol% Tm^{3+}/6 mol% Tb^{3+}/5 mol% Eu^{3+} phosphors.

average fluorescence lifetime (τ_{av}) can be performed using eqn (6):[41]

$$\tau_{avg} = \frac{A_1\tau_1^2 + A_2\tau_2^2}{A_1\tau_1 + A_2\tau_2} \quad (6)$$

The fluorescence lifetime decay curve of SNB:3 mol% Tm^{3+}, SNB:3 mol% Tm^{3+}, 6 mol% Tb^{3+} and SNB:3 mol% Tm^{3+}, 6 mol% Tb^{3+}, z Eu^{3+} phosphors is shown in Fig. 13 and the calculated τ_{av} value are 2.11, 1.90 and 1.64 ms, respectively. From the result it is evident that the decrement in the average life time of co doping sample SNB:3 mol% Tm^{3+}, 6 mol% Tb^{3} is due to energy transfer between Tm^{3+} to Tb^{3+}. Further, the average lifetime decreased further when it is doped with Eu^{3+}, thus powerfully confirming the existence of 3 mol% Tm^{3+} 6 mol% Tb^{3+} → z Eu^{3+}.

The CIE chromaticity coordinates of SNB:$x$$Tm^{3+}$, SNB:3 mol% Tm^{3+}, $y$$Tb^{3+}$ and SNB:3 mol% Tm^{3+}, 6 mol% Tb^{3+}, $z$$Eu^{3+}$ phosphors are evaluated using formulation from the reported work in literature[42,43]

$$CCT = -449n^3 + 3525n^2 - 6823.3n + 5520.33 \quad (7)$$

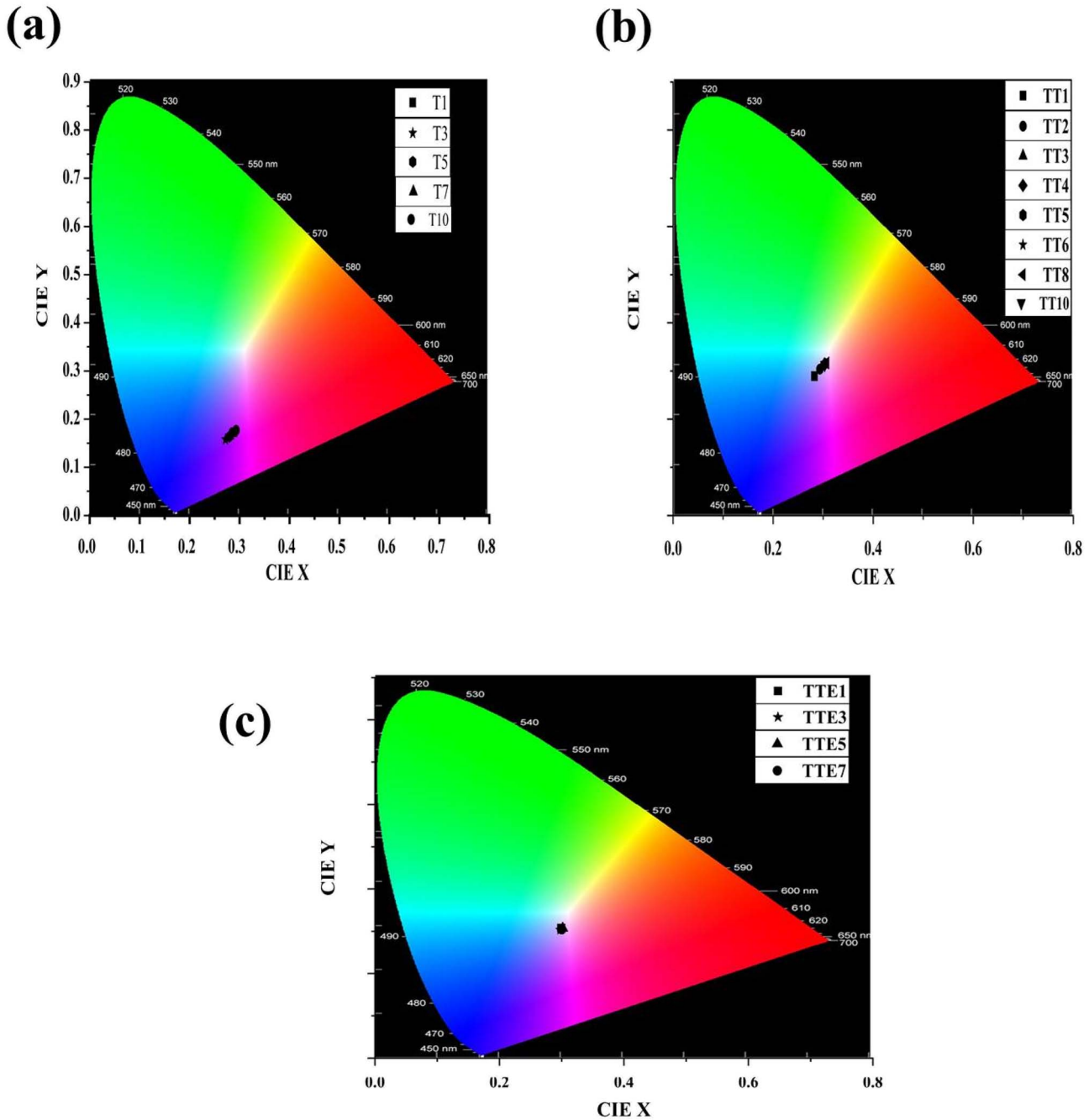

Fig. 14 CIE coordinates of (a) SNB:$x$$Tm^{3+}$, (b) SNB:3$Tm^{3+}$/$y$$Tb^{3+}$ and (c) SNB:3Tm^{3+}/6Tb^{3+}/$z$$Eu^{3}$ samples.

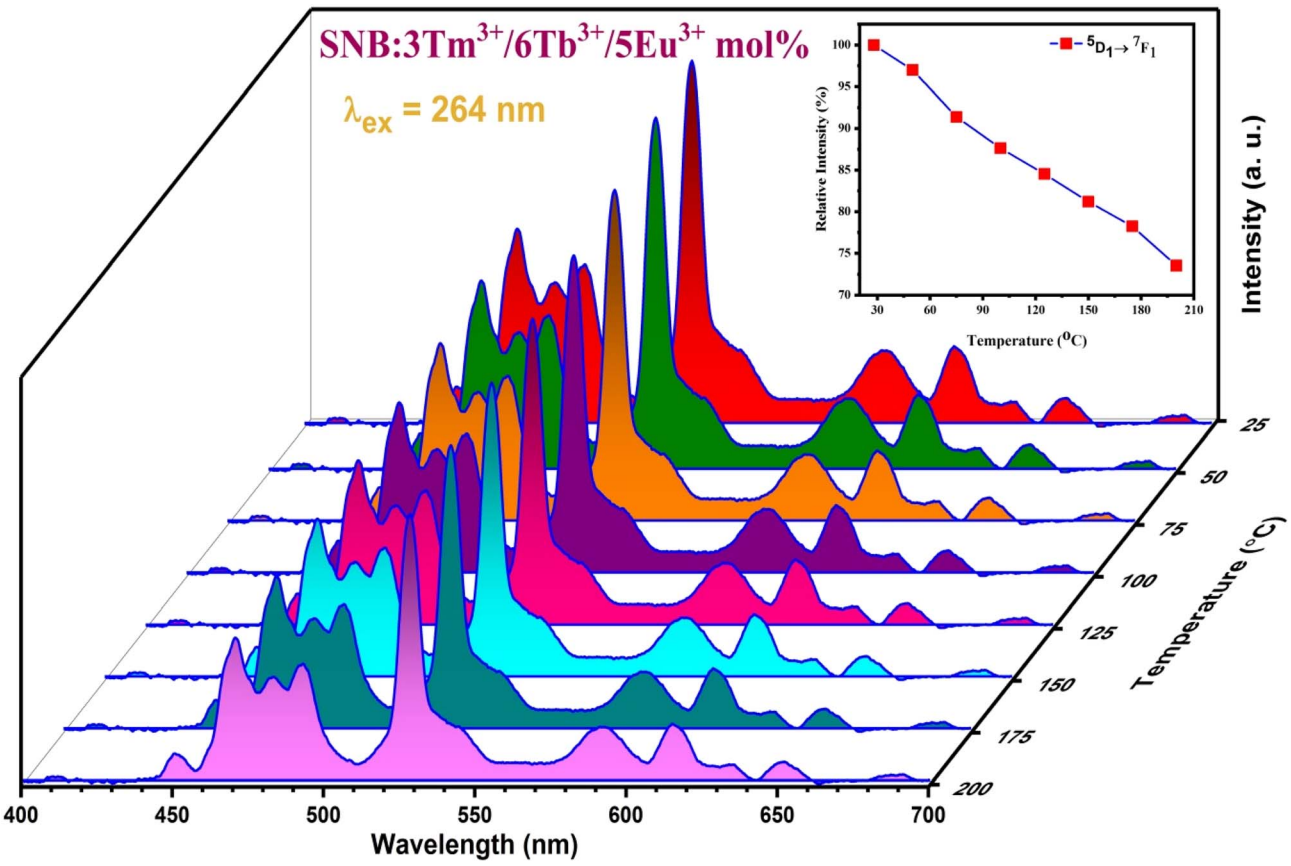

Fig. 15 TDPL spectra of SNB:3 mol% Tm^{3+}, 6 mol% Tb^{3+}, 5 mol% Eu^{3+} phosphor [inset exhibits the relative emission intensity variation for $^5D_1 \rightarrow {}^7F_1$ transition in the temperature range spanning from 28 to 200 °C].

and indicated in Table 1 and Fig. 14. These phosphors offer a remarkable avenue for color tunability, enabling the creation of customized illumination. The warm light can be achieved by adjusting the CCT and CRI values with NUV excitation of SNB:0.03Tm^{3+}, 0.06Tb^{3+}, zEu^{3+} phosphors. Notably, the CIE coordinates of TTE5 phosphor (0.3016, 0.3073) is close to standard value (0.31006, 0.3136). As highlighted in Table 1, increasing the concentration of Eu^{3+} concentration in the codoped phosphors has the effect of modifying the color temperature and enhancing the color rendering index by introducing the red emission into the spectra of white light. TTE1 phosphor represents the CCT of 7623 K and CRI 89.34 while the TTE3 phosphor emits the 7815 K CCT and 88.87 CRI white light. The result reveals that the TTE5 phosphor with higher Eu^{3+} concentration emits the cool light with CCT value of 7467 K and CRI value of 89.12. Hence, the white light with alterable CCT (7467–7815 K) and high CRI (>88) can be achieved for SNB:0.03Tm^{3+}, 0.06Tb^{3+}, zEu^{3+} phosphors with the control of Eu^{3+} concentration. Obviously, the TTE5 phosphor yield neutral white light with CCT of 7467 K and CRI of 89.12 with CIE coordinates (0.3016, 0.3073). These attributes position these phosphors as a strong contender for single-phased phosphors, holding significant promise for advancing neutral white light-emitting diodes (w-LEDs) with tunable color characteristics.

The thermal stability of as-prepared phosphors is crucial parameter in the application of W-LEDs device as operating temperature may increase significantly after the constant working of device at high temperature. The temperature dependent photoluminescence of SNB:3 mol% Tm^{3+}, 6 mol% Tb^{3+}, 5 mol% Eu^{3+} phosphor under 263 nm excitation was conducted in the range spanning from room temperature (28 °C) to 200 °C is shown in Fig. 15. The results indicate that the emission intensities of the as-prepared sample decreases with the rise in temperature because of thermal quenching but position remains unaltered. This decrement is attributed to the non-radiative transitions, therefore rate of intensity reduction changes over different emission peaks. This characteristic maintains the color stability of the as-prepared phosphors which indicates their reliable performance. Thermal stability was determined through the ratio of emission intensity at particular temperature to that at room temperature. The emission trend of the transition $^5D_1 \rightarrow {}^7F_1$ is depicted in the inset of Fig. 15. The strength of intensity at 150 °C and 200 °C relative to that at room temperature comes out to be 81.19% and 73.51%, respectively which is higher than reported work in the literature.[28] The results indicate the excellent thermal stability of the as-prepared phosphor.

3.7. Conclusions

We have synthesized a series of single-phase SNB phosphors co-doped with Tm^{3+}, Tb^{3+}, and Eu^{3+} ions. XRD analysis of the SNB phosphor confirms the formation of cubic structure within the

Fm3m space group and its match with standard data from the JCPDS file. The quantum efficiency of TT6 phosphor found to be 91.3%. The TDPL spectra reveal that the PL intensity persists to 81.19% at 150 °C in compare to room temperature. Under an excitation wavelength of 360 nm, Tm^{3+} single-doped SNB samples exhibit blue luminescence, characterized by an initial increase followed by a subsequent decrease in luminescence intensity. The maximum intensity is reached at a 3 mol% doping concentration. Additionally, the photoluminescence emission spectra of SNB phosphors co-doped with Tm^{3+} and Tb^{3+} ions, excited at 263 nm, reveal a declining intensity of Tm^{3+} emissions alongside an increasing intensity of Tb^{3+} emissions. This shift in the behavior of Tm^{3+} and Tb^{3+} ion intensities signifies the occurrence of energy transfer from Tm^{3+} to Tb^{3+} ions. Upon doping Eu^{3+} ions into the optimized co-doped sample (3 mol% Tm^{3+} and 6 mol% Tb^{3+}), both Tb^{3+} and Tm^{3+} ion intensities decrease as the concentration of Eu^{3+} ions increases. This variation in intensity is attributed to the energy transfer process from the optimized co-doped sample to Eu^{3+} ions. By carefully adjusting the doping concentrations of Tm^{3+}, Tb^{3+}, and Eu^{3+} ions to approximately 3 mol%, 6 mol%, and 5 mol%, respectively, the emission color can be fine-tuned to achieve white light emission.

Author contribution

Ravina: conceptualization, methodology, writing – original draft. Kanishk Poria: conceptualization, methodology, writing – original draft. Mukesh K Sahu: data curation, writing – review & editing. A. Kumar: formal analysis. Anu: formal analysis. Sajjan Dahiya: resources, formal analysis. Nisha Deopa: supervision, methodology, software, validation, writing – review & editing formal analysis. A. S. Rao: writing – review & editing.

Conflicts of interest

There are no conflicts to declare.

Acknowledgements

One of the authors, Ms Anu is very much thankful to CSIR/UGC for the award of a Junior Research Fellowship (JRF) (UGC Ref. 1352: CSIR-UGC NET DEC. 2018) to her.

References

1 J. Zheng, X. Wu, Q. Ren, W. Bai, Y. Ren, M. Wang and O. u. Hai, Investigation of luminescence properties and energy transfer in Sm^{3+} and Eu^{3+} co-doped $Sr_3Y(BO_3)_3$ red phosphors, *Opt. Laser Technol.*, 2020, **122**, 105857.

2 W. Zhang, H. Shen, X. Hu, Y. Wang, J. Li, Z. J. Zhu, Z. You and C. Tu, Solid-state synthesis, structure and spectroscopic analysis of Dy:$CaYAl_3O_7$ phosphors, *J. Alloys Compd.*, 2019, **781**, 255–260.

3 Q. Ren, Y. Zhao, X. Wu and O. Hai, Tb^{3+}/Eu^{3+}/Tm^{3+} co-doped single-phase phosphors emitting close to standard white light, *Opt. Laser Technol.*, 2021, **136**, 106774.

4 H. Patnam, S. K. Hussain, L. K. Bharat and J. S. Yu, Synthesis and luminescence properties of Eu^{3+} and Dy^{3+} ions single and co-doped $Ba_2LaV_3O_{11}$ phosphors for white-light applications, *Dyes Pigm.*, 2019, **162**, 583–589.

5 D. Rajesh, K. Brahmachary, Y. C. Ratnakaram, N. Kiran, A. P. Baker and G.-G. Wang, Energy transfer based emission analysis of Dy $^{3+}$/Eu $^{3+}$ co-doped ZANP glasses for white LED applications, *J. Alloys Compd.*, 2015, **646**, 1096–1103.

6 J. Li, H. Yan and F. Yan, A novel high color purity blue-emitting phosphor: $CaBi_2B_2O_7$: Tm^{3+}, *Mater. Sci. Eng., B*, 2016, **209**, 56–59.

7 T. S. Atabaev, H. H. Thi Vu, H. K. Kim and Y. H. Hwang, The optical properties of Eu^{3+} and Tm^{3+} codoped Y_2O_3 submicron particles, *J. Alloys Compd.*, 2012, **525**, 8–13.

8 G. Zhu, Z. P. Ci, Y. R. Shi, M. D. Que, Q. Wang and Y. H Wang, Synthesis, Crystal Structure and Luminescence Characteristics of a Novel Red Phosphor $Ca_{19}Mg_2(PO_4)_{14}$:Eu^{3+} for Light Emitting Diodes and Field Emission Displays, *J. Mater. Chem. C*, 2013, **1**, 5960–5969.

9 A. G. Bispo Jr, S. A. M. Lima and A. M. Pires, Energy transfer between terbium and europium ions in barium orthosilicate phosphors obtained from sol-gel route, *J. Lumin.*, 2018, **199**, 372–378.

10 P. C. Ricci, M. Salis, R. Corpino, C. M. Carbonaro, E. Fortin and A. Anedda, A Kinetics Model for Tb^{3+} Recombinations in Low Doped Tb:$Lu_{1.8}Y_{0.2}SiO_5$ Crystals, *J. Appl. Phys.*, 2010, **108**, 043512.

11 W. Zhao, X. Feng and B. Fan, Novel color tunable phosphors $NaYGeO_4$: Tm^{3+},Tb^{3+},Eu^{3+} for ultraviolet excited white LEDs with good thermal stability, *J. Mater. Sci.: Mater. Electron.*, 2020, **31**, 14434–14442.

12 V. V. Atuchin, B. I. Kidyarov and N. V. Pervukhina, Shortest chemical bond length as a criterion for searching new noncentrosymmetric niobate and tantalite crystals with high optical nonlinearity, *J. Cryst. Growth*, 2005, **275**, 1941–1946.

13 V. V. Atuchin, J. C. Grivel, A. S. Korotkov and Z. Zhang, Electronic parameters of $Sr_2Nb_2O_7$ and chemical bonding, *J. Solid State Chem.*, 2008, **181**, 1285–1291.

14 A. K. Vishwakarma, K. Jha, M. Jayasimhadri, A. S. Rao, K. Jang, B. Sivaiah and D. Haranath, Red light emitting $BaNb_2O_6$:Eu^{3+} phosphor for solid state lighting applications, *J. Alloys Compd.*, 2015, **622**, 97–101.

15 R. Lohan, A. Kumar, M. K. Sahu, A. Mor, V. Kumar, N. Deopa and A. S. Rao, Structural, thermal, and luminescence kinetics of $Sr_4Nb_2O_9$ phosphor doped with Dy^{3+} ions for cool w-LED applications, *J. Mater. Sci.: Mater. Electron.*, 2023, **34**, 694.

16 L. Alexander and H. P. Klug, Determination of crystallite size with the x-ray spectrometer, *J. Appl. Phys.*, 1950, **21**, 137–142.

17 M. Sharma, D. Kumar, J. P. Gewali and A. Thakur, Yttrium doped strontium nano hexaferrites: Influence of yttrium on the structural and magnetic properties of sol-gel synthesized nanocrystalline strontium hexaferrite, *Int. J. Mod. Phys.: Conf. Ser.*, 2022, **2267**, 012024.

18 K. Poria, R. Lohan, S. Bhatia, A. Kumar, R. Singh, N. Deopa, R. Punia, J. S. Shahi and A. S. Rao, Lumino-structural properties of Dy^{3+} activated $Na_3Ba_2LaNb_{10}O_{30}$ phosphors with enhanced internal quantum yield for w-LEDs, *RSC Adv.*, 2023, **13**(17), 11557–11568.

19 F. A. Kerim, H. F. Aly and A. Agramy, Infrared absorption spectra of some lanthanide acetylacetonate complexes, *Proc. Indian Acad. Sci.*, 1977, **85**, 559–566.

20 M. Afqir, A. Tachafine, D. Fasquelle, M. Elaatmani, J. C. Carru, A. Zegzouti, M. Daoud, S. Sayouri, T. D. Lamcharfi and M. Zouhairi, Structural, electric and dielectric properties of Eu-doped $SrBi_2Nb_2O_9$ ceramics obtained by co-precipitation route, Process, *Appl. Ceram.*, 2012, **12**, 72–77.

21 I. P. Sahu, D. P. Bisen, N. Brahme and R. K. Tamrakar, Generation of white light from dysprosium-doped strontium aluminate phosphor by a solid-state reaction method, *J. Mater. Sci.: Mater. Electron.*, 2016, **45**, 2222–2232.

22 W. T. Carnall, P. R. Fields and K. Rajnak, Electronic Energy Levels in the Trivalent Lanthanide Aquo Ions. I. Pr^{3+}, Nd^{3+}, Pm^{3+}, Sm^{3+}, Dy^{3+}, Ho^{3+}, Er^{3+}, and Tm^{3+}, *J. Chem. Phys.*, 1968, **49**, 4424.

23 W. T. Carnall, P. R. Fields and K. Rajnak, Electronic Energy Levels of the Trivalent Lanthanide Aquo Ions. III. Tb^{3+}, *J. Chem. Phys.*, 1968, **49**, 4447.

24 M. Wang, Y. Zhang, Z. Hu and J. Zhang, A single-phased $Ca_4(PO_4)_2O$: Tm^{3+}, Tb^{3+}, Eu^{2+} white light-emitting phosphor with tunable emission color, *J. Lumin.*, 2020, **224**, 117301.

25 W. Xiulan, D. Liang, Y. Zheng, M. Pei, Q. Ren and O. Hai, $Tm^{3+} \rightarrow Tb^{3+}$ energy transfer induced color-tunable in double-doped $LiLaSiO_4$ phosphors, *J. Lumin.*, 2021, **235**, 118027.

26 N. Deopa and A. S. Rao, Spectroscopic studies of single near ultraviolet pumped Tb^{3+} doped Lithium Lead Alumino Borate glasses for green lasers and tricolour w-LEDs, *J. Lumin.*, 2018, **194**, 56–63.

27 R. Pillania, A. Prasad, P. Rohilla, A. Shandilya and A. S. Rao, Photoluminescence and energy transfer studies on Tm^{3+}/Dy^{3+}/Eu^{3+}doped borosilicate glasses for color tunability and warm white light generation, *J. Non-Cryst. Solids*, 2023, **606**, 122192.

28 X. Wu, W. Bai, O. Hai, Q. Ren, J. Zheng and Y. Ren, Tunable color of Tb^{3+}/Eu^{3+}/Tm^{3+}-coactivated $K_3La(PO_4)_2$ via energy transfer: A single-phase white-emitting phosphor, *Opt. Laser Technol.*, 2019, **115**, 176–185.

29 X. Wu, L. Du, Y. Zheng, M. Pei, Q. Ren and O. Hai, $Tm^{3+} \rightarrow Tb^{3+}$ energy transfer induced color-tunable in double-doped $LiLaSiO_4$ phosphors, *J. Lumin.*, 2021, **235**, 118027.

30 X. Liu, C. Chen, S. Li, Y. Dai, H. Guo, X. Tang, Y. Xie and L. Yan, Host-sensitized and tunable luminescence of $GdNbO_4$: Ln^{3+} (Ln^{3+}= Eu^{3+}/Tb^{3+}/Tm^{3+}) nanocrystalline phosphors with abundant color, *Inorg. Chem.*, 2016, **55**, 10383–10396.

31 Y. Chen, X. Liu, G. Chen, T. Yang and C. Yuan, Luminescent characteristics of Tm^{3+}/Tb^{3+}/Eu^{3+} tri-doped borophosphate glasses for LED applications, *J. Mater. Sci.: Mater. Electron.*, 2017, **28**, 5592–5596.

32 Z. Wang, H. Tang, J. Xie, X. Zhang, X. Liu, X. Mi, Q. Liu, L. Lu and Z. Bai, Tunable color and energy transfer of $Y_2Mg_3Ge_3O_{12}$: Tb^{3+}, Tm^{3+}, Eu^{3+} phosphors with excellent thermal stability, *J. Solid State Chem.*, 2022, **314**, 123371.

33 H. Thakur, A. K. Gathania, I. Kumar and R. K. Singh, Tunable white light photoluminescence of a single phase Tm^{3+}/Tb^{3+}/Eu^{3+} codoped $GdPO_4$ phosphor, *Mater. Today Commun.*, 2023, **36**, 106458.

34 G. Blasse and B. C. Grabmaier, *Energy Transfer in Luminescent Materials*, Springer Berlin Heidelberg, Berlin, Heidelberg, 1994, pp. 91–107.

35 G. Blasse, Energy transfer in oxidic phosphors, *Philips Res. Rep.*, 1969, **24**, 131–144.

36 K. Li, M. Shang, H. Lian and J. Lin, Recent development in phosphors with different emitting colors via energy transfer, *J. Mater. Chem. C*, 2016, **24**, 5507–5530.

37 J. Xiong, Q. Meng and W. Sun, Luminescent properties and energy transfer mechanism from Tb^{3+} to Eu^{3+} in $CaMoO_4$:Tb^{3+},Eu^{3+} phosphors, *J. Rare Earths*, 2016, **34**, 251–258.

38 D. L. Dexter, A theory of sensitized luminescence in solids, *J. Chem. Phys.*, 1953, **21**, 836–850.

39 C. H. Huang, T.-W. Kuo and T.-M. Chen, Novel Red-Emitting Phosphor $Ca_9Y(PO_4)_7$:Ce^{3+},Mn^{2+} with Energy Transfer for Fluorescent Lamp Application, *ACS Appl. Mater. Interfaces*, 2010, **2**, 1395–1399.

40 N. Deopa, M. K. Sahu, P. R. Rani, R. Punia and A. S. Rao, Realization of warm white light and energy transfer studies of Dy^{3+}/Eu^{3+} co-doped Li_2O-PbO-Al_2O_3-B_2O_3 glasses for lighting applications, *J. Lumin.*, 2020, **222**, 117166.

41 Y. Zhu, Q. Meng, W. Sun and S. Lü, $NaLa(MoO_4)_2$: Sm^{3+}, Tb^{3+} phosphor: optical temperature sensing material with a wide change range of luminescence color, *J. Lumin.*, 2020, **218**, 116854.

42 A. Kumar, A. Mor, M. K. Sahu, R. Pillania, S. Dahiya, N. Deopa, A. Malik, R. Punia and A. S. Rao, Spectral characteristics of Tb^{3+} doped ZnF_2–K_2O–Al_2O_3–B_2O_3 glasses for epoxy free tricolor w-LEDs and visible green laser applications, *J. Lumin.*, 2022, **244**, 118676.

43 C. S. McCamy, Correlated color temperature as an explicit function of chromaticity coordinates, *Color Res. Appl.*, 1992, **17**, 142–144.